

MID-INFRARED SPECTRA OF CLASS I PROTOSTARS IN TAURUS

DAN M. WATSON,¹ F. KEMPER,² NURIA CALVET,³ LUKE D. KELLER,⁴ ELISE FURLAN,⁵ LEE HARTMANN,³ W. J. FORREST,¹ C. H. CHEN,⁶
KEVEN I. UCHIDA,⁵ JOEL D. GREEN,¹ B. SARGENT,¹ G. C. SLOAN,⁵ TERRY L. HERTER,⁵ BERNHARD R. BRANDL,⁷ J. R. HOUCK,⁵
J. NAJITA,⁸ PAOLA D’ALESSIO,⁹ P. C. MYERS,³ D. J. BARRY,⁵ P. HALL,⁵ AND P. W. MORRIS¹⁰

Received 2004 April 8; accepted 2004 May 26

ABSTRACT

We present *Spitzer Space Telescope* Infrared Spectrograph observations in the 5.3–20 μm range of five young stellar objects in Taurus that have Class I continuum spectral energy distributions ($\lambda F_{\lambda} \propto \lambda^n$, $n \geq 0$), often taken to represent the youngest stellar objects in this star formation region. The spectra include a rich collection of broad absorption features that we identify with amorphous silicates and various ices, notably those of carbon dioxide and water. We show that the absorption features are produced mainly in the envelopes of these systems. The apparent depths of silicate and 15.2 μm CO₂ ice features vary among the objects in a manner that is consistent with a variation of inclination with respect to the line of sight, contribution to the silicate features from material throughout the envelopes, and an origin for the CO₂ ice feature in the outer parts of the envelope. Thus, these features provide new and useful constraints on models of the physical structure of Class I protostars.

Subject headings: accretion, accretion disks — circumstellar matter — infrared: stars — stars: formation — stars: pre-main-sequence

Online material: color figures

1. INTRODUCTION

Among some three hundred pre-main-sequence objects in the Taurus-Auriga star-formation regions that were observed at infrared wavelengths by *IRAS* (Beichman et al. 1986, 1992; Myers et al. 1987; Kenyon et al. 1994), about a tenth are Class I protostars. This type of young stellar object (YSO) is defined by an extremely red energy spectrum at near- and mid-infrared wavelengths ($\lambda F_{\lambda} \propto \lambda^n$, $n \geq 0$) and little evidence for stellar photospheric emission at shorter wavelengths (Adams et al. 1987). Members of the class are also commonly associated with bipolar molecular outflows (e.g., Plambeck et al. 1983), jets and Herbig-Haro objects (e.g., Edwards et al. 1993), and bipolar infrared reflection nebulosity (e.g., Padgett et al. 1999). In addition, mass accretion rates in the optically thick disks of Class I objects have been determined (Muzerolle et al. 1998) to be roughly an order of magnitude larger than the average rates in classical T Tauri stars. These characteristics of extreme youth have been used, along with the small fraction of Class I among the YSO population, in a conventional description of Class I objects as the youngest members of the Taurus-Auriga

stellar associations: stars surrounded by optically thick disks and substantial envelopes, still in the process of accretion of a significant fraction of their final masses, and no more than a few hundred thousand years of age (Adams et al. 1987; Hartmann 1998).

Our present understanding of the details of the structure of Class I objects—and therefore of the infancy and formative years of young stars and planetary systems—is based upon the application of sophisticated models (e.g., Whitney et al. 2003a, 2003b; Osorio et al. 2003; Kenyon et al. 1993; Adams et al. 1987) to *IRAS* and ground-based, broadband, mid- and far-infrared observations of these objects’s continuum spectral energy distribution (SED), illuminated occasionally by high-resolution images of their jets and scattered light by cameras on the *Hubble Space Telescope* (*HST*). It has long been recognized that the mid-infrared range also contains narrow spectral features of dust and gas that carry much more detailed information about the structure and physical state of these objects. With the advent of the *Spitzer Space Telescope* (Werner et al. 2004), the mid-infrared spectra of large numbers of faint, low-mass YSOs are within our grasp. We report in this paper mid-infrared spectra of low-mass Class I objects in the Taurus association and show that these spectra bear strong absorption features from dust dominated by different physical regimes in these systems.

2. OBSERVATIONS

We observed five Class I targets in the Taurus dark cloud region on 2004 February 6–8, using the *Spitzer* Infrared Spectrograph¹¹ (IRS; Houck et al. 2004). All five are members of the Taurus YSO association, the distance to which we take to be 140 pc. A journal of the observations appears in Table 1. We chose our targets from the list by Kenyon & Hartmann (1995).

¹ Department of Physics and Astronomy, University of Rochester, Rochester, NY 14627-0171; dmw@pas.rochester.edu.

² *Spitzer* Fellow, Department of Physics and Astronomy, University of California, Los Angeles, CA 90095-1562.

³ Harvard-Smithsonian Center for Astrophysics, 60 Garden Street, Cambridge, MA 02138.

⁴ Department of Physics, Ithaca College, Ithaca, NY 14850.

⁵ Center for Radiophysics and Space Research, Cornell University, Space Sciences Building, Ithaca, NY 14853-6801.

⁶ National Research Council Resident Research Associate, Jet Propulsion Laboratory, MC 169-506, California Institute of Technology, 4800 Oak Grove Drive, Pasadena, CA 91109.

⁷ Sterrewacht Leiden, P.O. Box 9513, 2300 RA Leiden, Netherlands.

⁸ National Optical Astronomy Observatory, 950 North Cherry Avenue, Tucson, AZ 85719.

⁹ Centro de Radioastronomía y Astrofísica, UNAM, Apartado Postal 3-72 (Xangari), 58089 Morelia, Michoacán, Mexico.

¹⁰ *Spitzer* Science Center/Infrared Processing and Analysis Center, California Institute of Technology, Pasadena, CA 91125.

¹¹ The IRS was a collaborative venture between Cornell University and Ball Aerospace Corporation funded by NASA through the Jet Propulsion Laboratory and the Ames Research Center.

TABLE 1
OBSERVATION LOG

Name	Bolometric Luminosity (L_{\odot})	R.A. (J2000)	Decl. (J2000)	Observing Mode	<i>Spitzer</i> AOR Key
IRAS 04016+2610.....	3.7 ^a	04 04 43.07	+26 18 56.4	SL-SH spectral map	0003528960
IRAS 04108+2803B.....	0.6 ^a	04 13 54.72	+28 11 32.9	SL-SH spectral map	0003529472
IRAS 04181+2654B.....	0.3 ^a	04 21 10.39	+27 01 37.3	SL-LL staring	0003545856
IRAS 04239+2436.....	1.3 ^a	04 26 56.30	+24 43 35.3	SL-SH spectral map	0003530752
DG Tau B.....	0.7 ^b	04 27 02.66	+26 05 30.5	SL-SH staring	0003540992

NOTE.—Units of right ascension are hours, minutes, and seconds, and units of declination are degrees, arcminutes, and arcseconds.

^a Kenyon & Hartmann (1995).

^b This work.

Three of them appear to be single stars. Two, IRAS 04108+2803B and IRAS 04181+2654B, have apparent companions (visible in near-infrared observations) sufficiently distant to resolve completely in our spectral observations. Depending upon the anticipated brightness of each object, we operated the observatory either in IRS staring or IRS spectral mapping mode. We observed faint objects in Staring mode, in which a high-accuracy pointing peak-up, using the on-board Pointing Control Reference Sensor, was followed by exposures on the individual objects in both orders of the IRS short-wavelength, low-resolution spectrograph (Short-Low [SL]; 5.3–15 μm , $\lambda/\Delta\lambda \sim 90$), and either the IRS short-wavelength,

high-resolution spectrograph (Short-High [SH]; 10–19 μm , $\lambda/\Delta\lambda \sim 600$) or both orders of the long-wavelength, low-resolution spectrograph (Long-Low [LL]; 15–40 μm , $\lambda/\Delta\lambda \sim 90$), proceeding through the slits from short wavelengths to long. Each spectrograph and order was used for two observations, with the telescope nodded by one-third of the slit length in the spatial direction between consecutive exposures. In spectral mapping mode, the high accuracy peak-up is omitted; instead, a 2×3 raster (spatial \times dispersion) centered on the star is performed. The slit positions were separated by either three-quarters (for SL) or half (for other modules) their widths in the dispersion direction, and by a third of their length in the spatial direction.

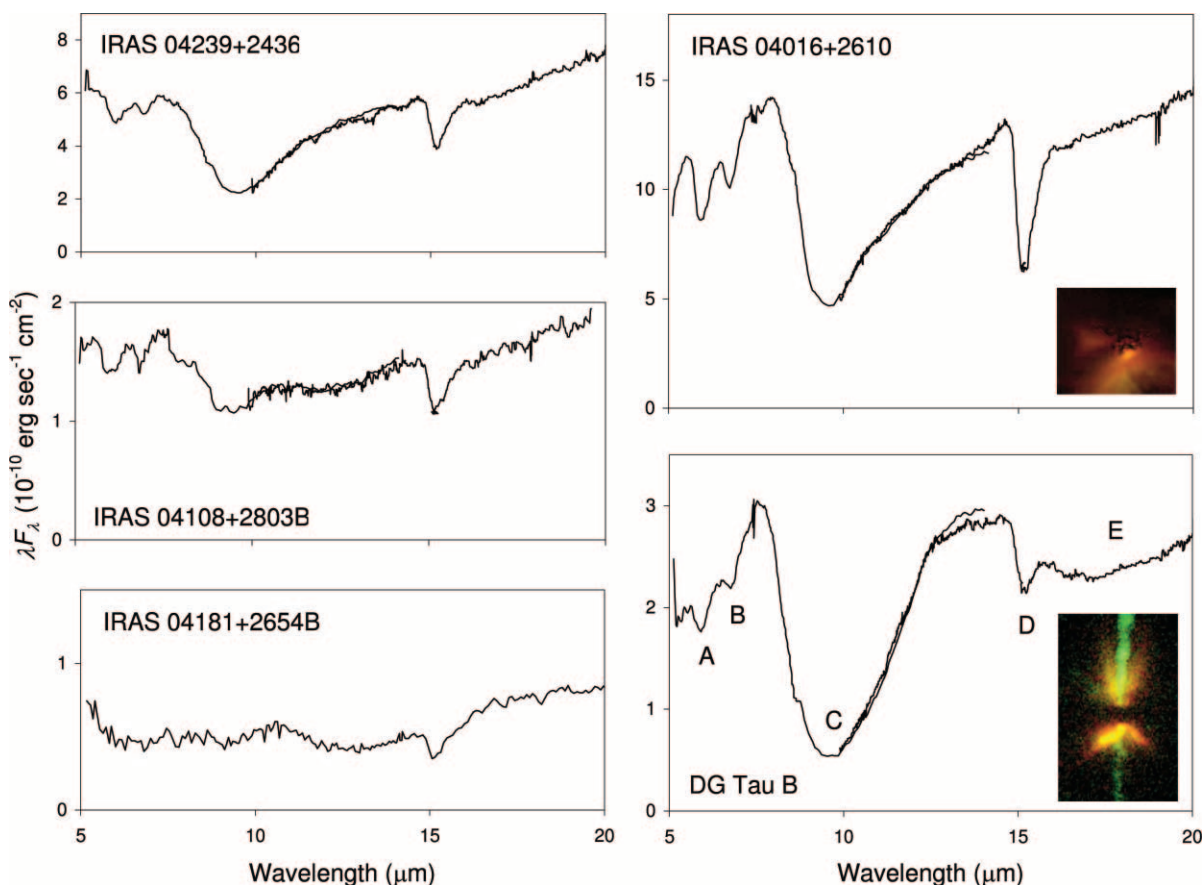


FIG. 1.—*Spitzer* IRS spectra of the present five Taurus Class I objects. The main spectral features of dust that we observe are labeled in the spectrum of DG Tau B: (A) water ice, (B) “methanol” ice, (C and E) amorphous silicates, and (D) carbon dioxide ice. In all the spectra except that of IRAS 04181+2654B, overlapping SL (5.3–14 μm) and SH (10–19 μm) spectra are shown, the latter median-smoothed to an effective resolving power of $\lambda/\Delta\lambda = 300$. Insets are *Hubble Space Telescope* images: a NICMOS image of IRAS 04016+2610 (Padgett et al. 1999) and a composite continuum and spectral-line image of DG Tau B taken with the WFPC2 instrument (Stapelfeldt et al. 1997).

We carried out the bulk of the reduction and analysis of our spectra with the IRS team’s SMART program (Higdon et al. 2004). We started with intermediate products from the *Spitzer* IRS data-reduction pipeline, that lacked only stray light and flat-fielding corrections. From the low spectral resolution data, we extracted point-source spectra for each nod position using a uniformly weighted column for which the variable width scales with the width of the instrumental point-spread function. Full-slit extractions were performed on the data from the high spectral resolution modules. We also made similar spectral extractions for observations of two photometric standard stars, α Lac (A1 V), and ξ Dra (K2 III). Then we divided each target spectrum, nod position by nod position, by the spectrum of one of the standard stars, multiplied the quotient by the appropriate template spectrum (Cohen et al. 2003), and averaged the resulting spectra from corresponding nod positions. In two cases—SL for IRAS 04108+2803B and LL for IRAS 04181+2654B—small (15%) wavelength-independent corrections were made to remove the effects of small telescope pointing variation. The resulting spectra of our five targets appear in Figure 1.

Based upon comparisons of our IRS spectra to ground-based flux densities, *IRAS* flux densities, and *Spitzer* IRAC flux densities of nonvariable calibration sources, we estimate that the absolute spectrophotometric accuracy of these spectra is 10% (1σ). This photometric accuracy also takes into account wavelength-independent interorder adjustments such as the two described above, which are necessary because of the current (and temporary) lack of flat-field correction at this early stage of *Spitzer*’s calibration. It is important to distinguish this absolute photometric accuracy, which describes the vertical positions of the spectra on our plots relative to the flux density scale, from the point-to-point fluctuation in the spectra, which is a measure of the precision of our spectral feature strengths and therefore of our ability to identify spectral features and compare them to our models. The accuracy of our spectral feature identifications and feature strengths is limited by the point-to-point scatter (currently much larger than system noise, in bright objects) that is visible in the spectra. Therefore, almost all features that significantly exceed the fluctuations and are wider than the 2 pixel IRS spectral resolution element are significant. All spectral features that we refer to in this paper meet these criteria.

3. ANALYSIS AND CONCLUSIONS

Superficially, the spectra in Figure 1 resemble those of embedded YSOs observed with *ISO* SWS and ISOCAM (e.g., Gibb et al. 2004; Alexander et al. 2003; Nummelin et al. 2001; Whittet et al. 1996). Strong features from amorphous silicates appear at 9.7 and 18 μm . These features appear purely in absorption for all except IRAS 04181+2654B, which shows the effects of emission and absorption in similar amounts. All the spectra also have strong absorptions by ices: CO_2 at 15.2 μm , H_2O at 6.0 μm , and a band at 6.8 μm often identified (but implausibly; see Gibb et al. 2004; Keane et al. 2001; Schutte et al. 1996) with CH_3OH . These features make the present spectra easily distinguishable from those of classical T Tauri stars in Taurus; we have seen no mid-infrared ice features in these latter objects, and not very many silicate absorption features, despite the appearance in some of the classical T Tau stars of mid-infrared continuum SEDs sufficiently red almost to fit the Class I description (Forrest et al. 2004).

However, they differ in detail from the *ISO* spectra, principally in that the ice features are very strong in the Class I

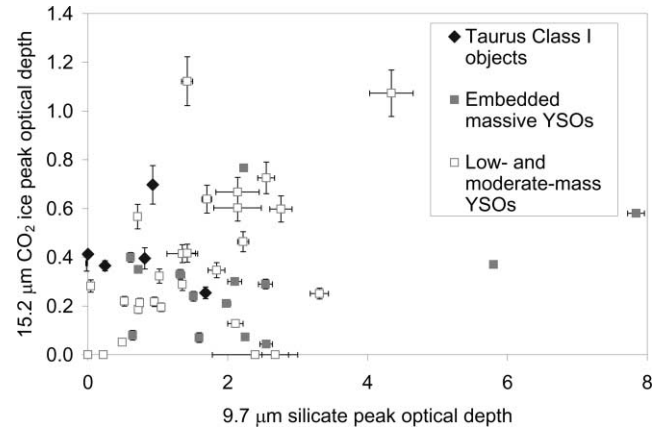


FIG. 2.—Apparent peak optical depth of the 15.2 μm CO_2 ice feature vs. that of the 9.7 μm silicate feature, for our Class I objects (diamonds) and for the embedded YSOs observed with *ISO* (filled squares, Gibb et al. 2004; empty squares, Alexander et al. 2003). To facilitate this comparison, we converted the 15.2 μm CO_2 ice equivalent widths reported by Alexander et al. to peak optical depths, using the ratio $2.24 \pm 0.2 \mu\text{m}^{-1}$ determined from our sample. [See the electronic edition of the *Journal* for a color version of this figure.]

objects. To illustrate this we plot in Figure 2 the apparent peak optical depth of the 15.2 μm CO_2 ice feature against that of the 9.7 μm silicate feature for the present five objects, and for the objects observed by Gibb et al. and Alexander et al. In this plot the Class I targets cover the same range of silicate optical depth as the bulk of the Gibb et al. sample, but all except DG Tau B lie higher in CO_2 ice feature strength. Alexander et al. observe 15.2 μm CO_2 ice features as strong as we detect, but typically for much larger silicate depth. This difference is likely to be due to significant contributions to the absorption features from foreground material in dense molecular-cloud surroundings, present for most of the objects observed by *ISO*, but weaker for objects within the relatively thin Taurus cloud. Rieke & Lebofsky (1985) derive $A_V/\tau_{\text{Si}} \approx 17$ for grains in the interstellar medium. This would indicate $A_V = 10\text{--}30$ for the present Class I objects, to compare with the general extinction determined toward Taurus association stars of $A_V = 1\text{--}5$ and the total extinction through the densest Taurus molecular-cloud cores of $A_V = 2\text{--}20$ (Myers et al. 1983). Only one of our targets (IRAS 04108+2803B) lies near a cloud core (L1495) dense enough that its silicate feature could be explained by a location on the far side and absorption by the intervening cloud; even if this were the case, the 15.2 μm CO_2 ice feature would still be unusually strong. The foreground and molecular-cloud extinguishing material can be inferred to have very weak absorption in the 15.2 μm CO_2 ice feature compared to what we observe, judging from observations of the 4.3 μm CO_2 feature in stars behind the Taurus clouds (Nummelin et al. 2001), and from *Spitzer* IRS observations of other Taurus association objects (Forrest et al. 2004). To first approximation, then, we can take the Taurus Class I objects to be unaffected by mid-infrared foreground absorption and can attribute the absorptions to the objects’s disks and envelopes.

The shape of the 15.2 μm CO_2 ice feature is a powerful probe of composition and temperature in ice-bearing dust grains. In our spectra the shape indicates that the composition of this ice is not very different from that in the lines of sight to the embedded, massive YSOs studied by Gibb et al. (2004). In Figure 3 we show as examples some fits to this feature in the spectrum of DG Tau B. In this process we used a foreground-screen absorber model, and the laboratory ice spectra measured

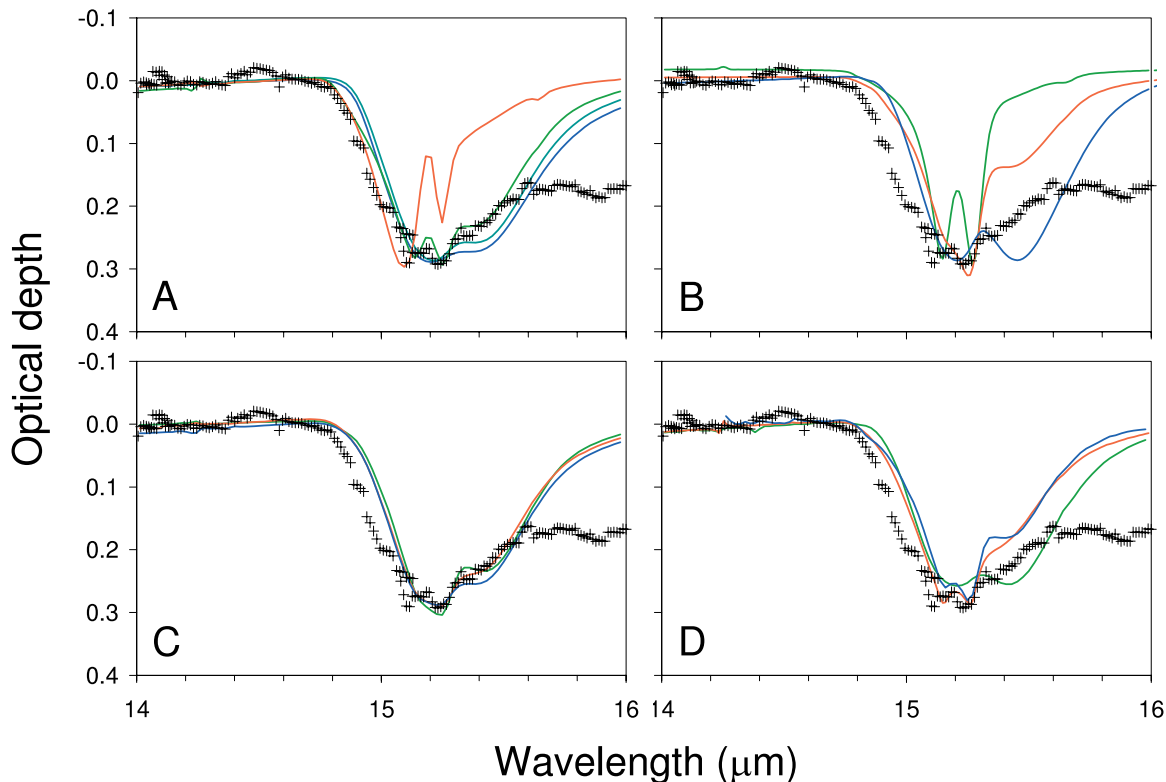


FIG. 3.—Fits to the $15 \mu\text{m}$ feature in DG Tau B, shown in crosses, with laboratory spectra of ices. Panel (a) contains spectra at several temperatures for a 1:1:1 (by mass fraction) mixture of water, methanol, and CO_2 ices: 10 K (blue line), 65 K (cyan line), 115 K (green line), and 120 K (red line). Panel (b) contains spectra of CO_2 - CH_3OH mixtures in the following ratios: CO_2 : CH_3OH = 10:1 (green line, 75 K), 3:1 (red line, 90 K), and 1:1 (blue line, 84 K). In (c) we show three of a large number of good fits that occur when H_2O is mixed in as well. The compositions shown are H_2O : CH_3OH : CO_2 = 0.2:0.6:1 (green line, 80 K), 0.7:0.7:1 (red line, 80 K), and 1:1:1 (blue line, 80 K). Finally, in (d) we show some H_2O : CH_3OH : CO_2 mixtures that do not lead to very good results. The mixtures are 0.6:1:0.8 (green line, 80 K), 1.2:0.7:1 (red line, 87 K), and 0.3:0.5:1 (blue line, 85 K).

by Ehrenfreund et al. (1999) for a range of temperatures and compositions expected in Class I envelopes. Polar ice mixtures give a reasonably good account of the observed shape of the core and long-wavelength wing of these features. The mixtures with the best fits are similar to those favored in typical fits to $15.2 \mu\text{m}$ CO_2 ice features by Gibb et al. (2004). Thus, the large strength of the $15.2 \mu\text{m}$ CO_2 ice features in Class I objects, relative to those of the objects studied by Gibb et al., is not related to ice-mantle composition. It is more likely to be the combined effect of a large dust column density in the envelope, and of the relatively low luminosity of the central star, in promoting an unusually large $15.2 \mu\text{m}$ CO_2 ice quantity per dust grain.

Silicate and ice features exhibit different trends in the spectra of the Taurus Class I objects. For simplicity we will illustrate this using the $9.7 \mu\text{m}$ silicate and $15.2 \mu\text{m}$ CO_2 ice features. The $9.7 \mu\text{m}$ silicate feature varies widely in apparent depth among the five targets, down to nearly zero. This is similar to expectations for Class I objects for different inclinations of the system's axis with respect to the line of sight, and significant contributions from throughout the envelope, as in the models by Kenyon et al. (1993) or Whitney et al. (2003a, 2003b): a silicate spectrum like that of IRAS 04181+2654B would correspond to a disk/envelope system viewed nearly face on, one like that of DG Tau B to a system nearly edge on (in nice accord with its *HST* image; see Fig. 2), and the rest of the spectra would correspond to intermediate cases of inclination (as is apparent in IRAS 04016+2610; see Fig. 2). The $15.2 \mu\text{m}$

CO_2 ice feature strength does not track that of the silicate feature; it is large and in absorption at all inclinations. This indicates an origin for this feature in the outer, more symmetrical, sector of the envelope. While consistent with the thermal structure of the envelope, this result is somewhat unexpected: CO_2 ice is thought to be produced from CO in grain mantles by radiative heating of the grains, so the unusually large amounts per grain that we see in the Class I objects might be expected in the less-symmetrical interiors of the envelopes.

A comparison with the structure of Class I objects bears this picture out. We have constructed a set of model Class I objects, similar to those by Kenyon et al. (1993) and Calvet et al. (1994). These models are simple in the sense that the only narrow spectral features in the dust grain opacity are the silicate (Draine & Lee 1984) and $15.2 \mu\text{m}$ CO_2 ice features (Ehrenfreund et al. 1999), and that the warm inner disk is omitted, leaving the star and the envelope. They include slowly rotating, infalling envelopes (Terebey et al. 1984), with parameters that fit most of the broadband SEDs of the Taurus Class I objects (Kenyon et al. 1993). These envelopes are nearly spherically symmetric at radii much larger than the centrifugal radius R_C , which we take to be 50 AU, and depart from spherical symmetry inside this radius as material falls onto the disk. The heating of matter in the envelope is set by the luminosity of the central object. The temperature is calculated from the radiative equilibrium condition, using the angle-averaged density, and the inclination-dependent flux is calculated from ray-by-ray integration of the

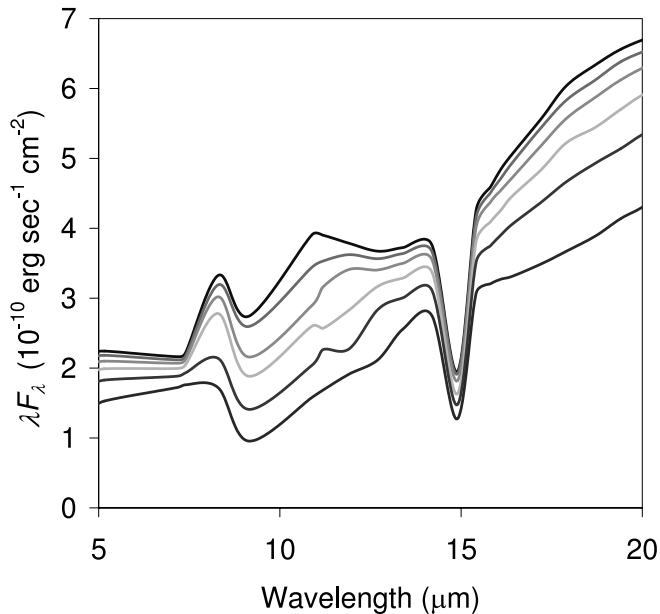


FIG. 4.—Mid-infrared spectra of a model Class I protostar, at distance 140 pc with luminosity $1 L_{\odot}$, as seen at different inclinations of the system axis with respect to the line of sight (top to bottom): 20° , 30° , 40° , 50° , 60° , and 70° . [See the electronic edition of the *Journal* for a color version of this figure.]

radiative-transfer equation using the angle-dependent density $\rho(r, \theta)$. The scattering component of the source function in the flux calculation is taken as the sum of the direct and diffuse mean intensities, following Calvet et al. (1994). The dust

components are similar to those adopted by Osorio et al. (2003), which fitted the SED of the (binary) Taurus Class I object L1551 IRS 5. Figure 4 is a plot of the $5\text{--}20 \mu\text{m}$ spectrum for models with axis inclination angles $20^{\circ}\text{--}70^{\circ}$ with respect to the line of sight. As usual, the silicate features in these models range from deep absorption to emission and absorption in comparable amounts, and vary accordingly in apparent depth. But the CO_2 ice feature always appears in absorption and varies in depth much less than the silicate feature, as the inclination varies.

Thus, ice features like that of CO_2 may allow us to separate, observationally, the contributions of different sectors to the appearance of Class I protostars. This is likely to place a new set of strong constraints on physical models of these systems, and in general on our picture of the evolution of stars and protoplanetary disks during the phase in which both disk accretion and stellar accretion are important.

We wish to thank our colleagues on the *Spitzer* project too numerous to list, and especially those on the IRS instrument team, for 21 years of hard and often frustrating work in getting the spectrograph and the observatory working so well. We are also grateful to David Whelan for help with the data reduction. The *Spitzer Space Telescope* is operated by the Jet Propulsion Laboratory, California Institute of Technology, under NASA contract 1407. Support for this work was provided by NASA through contract 1257184 issued by JPL/Caltech, and through the *Spitzer* Fellowship Program, under award 011 808-001.

REFERENCES

- Adams, F. C., Lada, C. J., & Shu, F. H. 1987, *ApJ*, 312, 788
 Alexander, R. D., Casali, M. M., André, P., Persi, P., & Eiroa, C. 2003, *A&A*, 401, 613
 Beichman, C. A., Boulanger, F., & Moshir, M. 1992, *ApJ*, 386, 248
 Beichman, C. A., Myers, P. C., Emerson, J. P., Harris, S., Mathieu, R., Benson, P. J., & Jennings, R. E. 1986, *ApJ*, 307, 337
 Calvet, N., Hartmann, L., Kenyon, S. J., & Whitney, B. A. 1994, *ApJ*, 434, 330
 Cohen, M., Megeath, S. T., Hammersley, P. L., Martín-Luis, F., & Stauffer, J. 2003, *AJ*, 125, 2645
 Draine, B. T., & Lee, H. M. 1984, *ApJ*, 285, 89
 Edwards, S., Ray, T., & Mundt, R. 1993, in *Protostars and Planets III*, ed. E. H. Levy & J. R. Lunine (Tucson: Univ. Arizona Press), 567
 Ehrenfreund, P., et al. 1999, *A&A*, 350, 240
 Forrest, W. J., et al. 2004, *ApJS*, 154, 443
 Gibb, E. L., Whittet, D. C. B., Boogert, A. C. A., & Tielens, A. G. G. M. 2004, *ApJS*, 151, 35
 Hartmann, L. 1998, *Accretion Processes in Star Formation* (New York: Cambridge Univ. Press)
 Higdon, S. J. U., et al. 2004, *PASP*, submitted
 Houck, J. R., et al. 2004, *ApJS*, 154, 18
 Keane, J. V., Tielens, A. G. G. M., Boogert, A. C. A., Schutte, W. A., & Whittet, D. C. B. 2001, *A&A*, 376, 254
 Kenyon, S. J., Calvet, N., & Hartmann, L. 1993, *ApJ*, 414, 676
 Kenyon, S. J., Gomez, M., Marzke, R. O., & Hartmann, L. 1994, *AJ*, 108, 251
 Kenyon, S. J., & Hartmann, L. 1995, *ApJS*, 101, 117
 Muzerolle, J., Hartmann, L., & Calvet, N. 1998, *AJ*, 116, 2965
 Myers, P. C., Fuller, G. A., Mathieu, R. D., Beichman, C. A., Benson, P. J., Schild, R. E., & Emerson, J. P. 1987, *ApJ*, 319, 340
 Myers, P. C., Linke, R. A., & Benson, P. J. 1983, *ApJ*, 264, 517
 Nummelin, A., Whittet, D. C. B., Gibb, E. L., Gerakines, P. A., & Chiar, J. E. 2001, *ApJ*, 558, 185
 Osorio, M., D'Alessio, P., Muzerolle, J., Calvet, N., & Hartmann, L. 2003, *ApJ*, 586, 1148
 Padgett, D. L., Brandner, W., Stapelfeldt, K. R., Strom, S. E., Terebey, S., & Koerner, D. 1999, *AJ*, 117, 1490
 Plambeck, R. L., Snell, R. L., & Loren, R. B. 1983, *ApJ*, 266, 321
 Rieke, G. H., & Lebofsky, M. J. 1985, *ApJ*, 288, 618
 Schutte, W. A., Tielens, A. G. G. M., Whittet, D. C. B., Boogert, A., Ehrenfreund, P., de Graauw, T., Prusti, T., van Dishoeck, E. F., & Wesseliuss, P. 1996, *A&A*, 315, L333
 Stapelfeldt, K., Burrows, C. J., Krist, J. E., & the WFPC2 Science Team. 1997, in *IAU Symp. 182, Herbig-Haro Flows and the Birth of Stars*, ed. B. Reipurth & C. Bertout (Dordrecht: Kluwer), 355
 Terebey, S., Shu, F. H., & Cassen, P. 1984, *ApJ*, 286, 529
 Werner, M. W., et al. 2004, *ApJS*, 154, 1
 Whitney, B. A., Wood, K., Bjorkman, J. E., & Cohen, M. 2003a, *ApJ*, 598, 1079
 Whitney, B. A., Wood, K., Bjorkman, J. E., & Wolf, M. J. 2003a, *ApJ*, 591, 1049
 Whittet, D. C. B., et al. 1996, *A&A*, 315, L357